EFFECT OF ADDING STEAM TO CH_4 DURING CHEMICAL LOOPING PROCESSES WITH Ni-BASED OXIGEN CARRIERS

Pedro H. L. N. A. dos Santos[1], Gilberto M. da Cruz[2], Livia M. Carneiro[3], Gustavo T. Moure[4], Marco A. Ferreira[5], José A. J. Rodrigues[6]

Abstract

The chemical-looping combustion (CLC) and chemical-looping reforming (CLR) processes allow combustion to take place in fuel gases such as CH_4 to generate energy and produce H_2, impeding the emission of CO_2 into the atmosphere and contributing to greenhouse mitigation. In this work, the effect of adding water steam to CH_4 was investigated, using $NiO/\alpha\text{-}Al_2O_3$ and $NiAl_2O_4/\gamma\text{-}Al_2O_3$ as oxygen carriers in order to reduce or eliminate the formation of carbon deposits on these materials when using long reductions steps. After characterizing the oxygen carriers using different techniques, they underwent many redox sequences, proving themselves to be stable. However, when CH_4 was employed as the only active component of the reaction mixture in argon, large carbon deposits were formed on both carriers. The carbon deposits were only removed by a subsequent oxidation step using oxygen in argon. In experiments carried out in which water steam was added to the CH_4 during the reduction step, carbon deposits on $NiAl_2O_4/\gamma\text{-}Al_2O_3$ were almost eliminated and on $NiO/\alpha\text{-}Al_2O_3$ were totally eliminated. Since the results were different, two different reaction mechanisms were proposed: the first in which the addition of H_2O impeded the formation of carbon deposits and the second in which the carbon formed was gasified by the water. Both of the mechanisms were evaluated thermodynamically and experimentally for each of the steps involved. It can be asserted that in the case of the $NiO/\alpha\text{-}Al_2O_3$ oxygen carrier, the second mechanism is much more probable since it involves quick and irreversible steps and in which water steam acts directly on the carbon deposits. In the case of the $NiAl_2O_4/\gamma\text{-}Al_2O_3$ carrier, both of the mechanisms are possible. Because they involve reversible reactions they don't result in the total elimination of carbon deposits, though the level of elimination is quite high.

1. Introduction

It is known that the release of greenhouse gas CO_2 to the atmosphere can affect the climate of the Earth. Most CO_2 released originates from burning fossil fuels (Lyngfelt et al., 2001).

The power industry is a major stationary source of CO_2, producing one-third of the world's CO_2 emissions from fossil fuel combustion (Lyngfelt et al.; 2001). It's possible that CO_2-free power generation would diminish the greenhouse effect. Today, sequestration of CO_2 mainly involves post-combustion processes in which there is a very high cost of separating CO_2 from the other flue gases (Zafar et al., 2006). After sequestration, CO_2 can be stored in different ways: storage in used oil and gas fields, deep saline aquifers, deep sea, and abandoned coal mines (Cunha and Santarosa, 2006).

Some processes have been studied as low cost alternatives to the conventional technologies. According to the IPCC (International Panel on Climate Change) and CCP (CO_2 Capture Project) chemical-looping combustion, CLC, is a

[1] Graduating, Chemical Engineer – Instituto Nacional de Pesquisas Espaciais
[2] Doctor, Chemical Engineer – Instituto Nacional de Pesquisas Espaciais
[3] Doctor, Chemical Bachelor – Instituto Nacional de Pesquisas Espaciais
[4] Master, Chemical Engineer – Petrobras
[5] Doctor, Chemical Engineer – Instituto Nacional de Pesquisas Espaciais
[6] Doctor, Chemical Engineer – Instituto Nacional de Pesquisas Espaciais

pre-combustion CO_2 capture process with low operating costs (Abad et al., 2007). This process utilizes two interconnected reactors: the first, the fuel reactor, is responsible for fuel combustion by a metal oxide called oxygen carrier. This partially-reduced carrier passes to the second reactor, the air reactor, where it is oxidized again and returns to the fuel reactor transporting the oxygen necessary for fuel combustion. In this way CO_2 is captured at the fuel reactor outlet without N_2 and no other separation method is necessary (Figure 1). In the fuel reactor, the oxygen carrier behaves as a bubbling fluid and in the air reactor it is carried out from the bottom to the top by a high volumetric air flow.

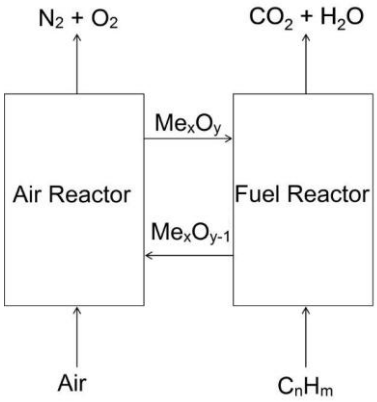

Figure 1. Diagram of a CLC interconnected reactor system.

A modification of CLC for the production of hydrogen with CO_2 capture is the chemical-looping reforming process (CLR), which has been suggested and investigated by several authors (Zafar et al., 2006; Rydén et al., 2008; Adanez et al., 2012). In this process, the oxygen carrier is used to provide the oxygen for the fuel to produce the syngas ($CO + H_2$), which is carried out to a third reactor (water-gas shift reactor) where the CO reacts with H_2O, being converted to CO_2 by a catalyst. The reactions that characterize the CLC (Equation 1) and CLR (Equation 2) processes at the fuel reactor with a generic metal oxide, Me_xO_y, and CH_4 as fuel are shown below.

$$CH_4 + 4Me_xO_y \rightarrow CO_2 + 2H_2O + 4Me_xO_{y-1} \quad (1)$$

$$CH_4 + Me_xO_y \rightarrow CO + 2H_2 + Me_xO_{y-1} \quad (2)$$

The chemical-looping system can be employed with both processes, depending on the metal oxide specification and operational conditions (Mattisson et al., 2003). At full conversion of the fuel gas, the exit gas stream contains only CO_2 and H_2O and these two components are easily separated by H_2O condensation. The reduced metal oxide, Me_xO_{y-1}, is then circulated to the air reactor where it is oxidized according to Equation 3.

$$Me_xO_{y-1} + \tfrac{1}{2}O_2 \rightarrow Me_xO_y \quad (3)$$

Steam or CO_2 could be added to the fuel to enhance the relative amount of steam reforming (Equation 4) or dry reforming (Equation 5) in the CLR process (Rydén et al., 2008).

$$CH_4 + H_2O \rightarrow CO + 3H_2 \quad (4)$$

$$CH_4 + CO_2 \rightarrow 2CO + 2H_2 \quad (5)$$

An oxygen carrier is normally made up of a metal oxide supported on an inert material with a high surface area, mechanical strength, and attrition resistance (Abad et al., 2007). Among the different metal oxides, Fe_2O_3 and Mn_3O_4 are inexpensive materials but presents low reactivity. CuO is very reactive but cannot be employed at high temperatures due to its low melting point (1085 °C). Despite their higher cost, oxygen carriers containing Ni have been studied in greater detail because their characteristics are more favorable for chemical-looping combustion (Wall et al. 2007). Ni-based carriers have good redox, thermodynamic, and mechanical properties and relatively high chemical stability. They also seem to have the highest reduction rate among others transitional metal oxygen carriers (Zafar at al.,

2006). Bench-scale results indicate Ni-based carriers are quite suitable for full combustion and partial oxidation of methane reforming at temperatures between 850-950 °C (Wall et al. 2007).

One of the greater problems with CLC/CLR processes is the fact that CH_4 can be decomposed, thermally or catalyzed by the oxygen carrier, generating H_2 and carbon, which is deposited on the carrier surface contributing to its deactivation. This carbon is oxidized in the air reactor, generating CO_2 or CO, which are released on the reactor outlet, decreasing the process efficiency (Adanez et al., 2012). The aim of this work was to investigate the behavior of two different oxygen carriers, NiO/α-Al_2O_3 and NiO/γ-Al_2O_3, submitted to combustion or reforming of methane and carry out a more detailed evaluation of adding steam to the reaction mixture, studied by several authors, as a way to eliminate the carbon deposition during the reduction step (Cho et al., 2004; Rydén et al., 2008; Gayán et al., 2008).

2. Experimental

2.1. Preparation of oxygen carriers

Two Ni-based oxygen carriers were prepared by impregnation of two different commercial aluminum oxide supports with $Ni(NO_3)_2.6H_2O$. The A1 support was characterized as γ-alumina and the A2 support was characterized as α-alumina. Both were from ALCOA.

The 9%NiO/γ-Al_2O_3 was prepared by wet impregnation of the γ-alumina (A1) with $Ni(NO_3)_2 . 6H_2O$ in one step and calcined at 950 ºC for 1 h. The 9%NiO/α-Al_2O_3 was prepared by dry impregnation of the α-alumina (A2) with $Ni(NO_3)_2 . 6H_2O$ in two steps and calcined at 950 ºC for 1 h, after each step.

2.2. Characterization

Several techniques were used to physically and chemically characterize the supports and oxygen carriers. The pore volumes (V_P) of the materials were determined by mercury porosimetry (Quantachrome PoreMaster 33 GT), specific surface areas (S) were determined by nitrogen adsorption (BET method using a Quantachrome Nova 2200e), nickel contents (%) were determined by atomic emission spectrometry (ICP/AES), and the crystalline phases of the materials were identified using powder method x-ray difratometry analysis (XRD). The TPR analysis (Temperature Programmed Reduction) of the oxygen carriers were carried out using a Quantachrome ChemBET 3000 with a gaseous mixture of 5% H_2/N_2 to determine the reduction temperature of the materials.

2.3. Reactivity tests by TGA (Thermogravimetric Analysis)

TGA reactivity tests were carried out to analyse oxygen weight during a sequence of oxidation and reduction cycles. Reactivity tests were carried out at 950 ºC with a total volumetric flow of 80 mL/min and oxygen carrier weight of approximately 50 mg. A molar concentration of 10% CH_4 was used in the reduction step and 20% O_2 was used in the oxidation step. Both were diluted with Ar. To avoid mixing CH_4 and O_2, Ar was introduced for five minutes after each reducing and oxidizing step.

Some important results obtained with these analyses were the oxygen carrier stability during the cycles, the rate of reduction and oxidation of the carriers and the consumption of available oxygen.

2.4. Fixed bed batch tests

The tests were carried out in a single fixed bed reactor to evaluate the gas product distribution during reduction and oxidation steps and selectivity of the materials for CLC or CLR processes. The tests were carried out at 950 ºC with total volumetric flow of 50 mL/min and oxygen carrier weight of approximately 1 g. Molar concentration of 10% CH_4 or 5% CH_4+5% H_2O were used in the reduction step and 20% O_2 was used in the oxidation step. Both were diluted with Ar. The reduction tests were carried out for 6 minutes and oxidation tests were carried out for 4 minutes for 10% CH_4 and 3 minutes for 5% CH_4+5% H_2O. To avoid mixing CH_4 and O_2, Ar was introduced for around ten minutes after each reducing and oxidizing step.

Tests to evaluate the mechanisms proposed in this work to explain the elimination or minimization of carbon deposition were carried out. The tests were conducted with 5% H_2 or 5% CO reacting with oxygen carriers and 5% H_2O reacting with reduced oxygen carriers or with carbon deposited on reduced oxygen carriers.

The tests were monitored by a MKS e-vision+ mass spectrometer and a Varian CP-3800 gas chromatograph. Figure 2 shows the experimental setup used for multicycle tests in a fixed bed reactor.

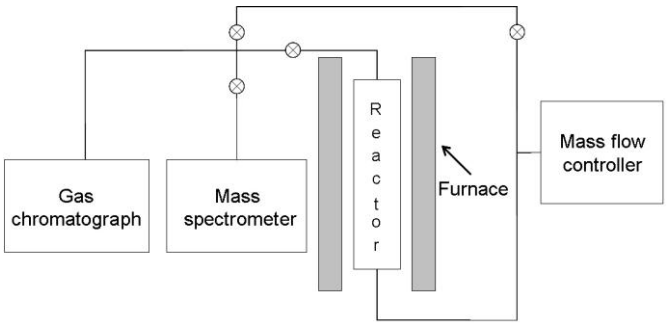

Figure 2. Experimental setup used for multicycle tests in a fixed bed reactor.

3. Results and Discussion

3.1. Characterization

Table 1 shows the characterization of the supports and oxygen carriers. Reduction of pore volumes can be seen after the impregnation of both supports, indicating that part of the NiO precursor was introduced into the pores of the two materials. With the 9%NiO/γ-Al_2O_3 carrier the surface specific area can be seen to diminish from 69 to 52 m^2/g, indicating the possibility that few pores were filled with NiO. With the 9%NiO/α-Al_2O_3 the introduction of the Ni precursor to the α-Al_2O_3 barely affected the surface specific area, which was already extremely reduced. The ICP results were very close to the theoretical values initially defined for the NiO content, which indicates a high yield for both impregnating methods. The XRD results indicate that 9%NiO/γ-Al_2O_3 has a $NiAl_2O_4$ active phase, justified by the reaction between NiO and γ-Al_2O_3 during the calcination treatment at 950 ºC. The 9%NiO/α-Al_2O_3 has only α-Al_2O_3 and NiO phases. Because of these results, the two oxygen carriers will be designated as NiO/α-Al_2O_3 and $NiAl_2O_4$/γ-Al_2O_3.

Table 1. Characterization of α-Al_2O_3, NiO/α-Al_2O_3, γ-Al_2O_3 and $NiAl_2O_4$/γ-Al_2O_3 showing V_P (pore volume), S (surface specific area), %Ni (ICP), %NiO* and crystalline phase (x-ray diffraction) results.

Material	V_P (cc/g)	S (m^2/g)	%Ni	%NiO*	XRD
γ-Al_2O_3	0.199	69	-		γ-Al_2O_3
9%NiO/γ-Al_2O_3	0.194	52	7.5	9.6	γ-Al_2O_3, $NiAl_2O_4$
α-Al_2O_3	0.266	2	-		α-Al_2O_3
9%NiO/α-Al_2O_3	0.223	2	6.6	8.4	α-Al_2O_3, NiO

*Theoretical values considering only the formation of NiO.

Figure 3 shows the TPR analysis of the two oxygen carriers: NiO/α-Al_2O_3 and $NiAl_2O_4$/γ-Al_2O. $NiAl_2O_4$/γ-Al_2O_3 has two different reduction temperature ranges, the first with low intensity between 550 and 600 ºC and the second, with higher intensity centered 780 ºC. According to Gayán et al. (2009), the first temperature range can be attributed to the NiO phase and the second to the $NiAl_2O_4$ phase. Unlike XRD analyses which showed only a $NiAl_2O_4$ phase for NiO/γ-Al_2O_3, the TPR analysis leads to the conclusion that the NiO phase, present in a small amount, may be very dispersed on the oxygen carrier, therefore the NiO spectrum could not be detected by this XRD. The NiO/α-Al_2O_3 oxygen carrier has two reduction peaks at 418 and 471 ºC. According to Gayán et al. (2009) peaks between 400 and 600 ºC represents the reduction of NiO to Ni^0, and the presence of two peaks can be attributed to different crystal sizes of the NiO or different degrees of interaction of Ni with the support. Thus it is possible to say that the TPR results agree with XRD analysis.

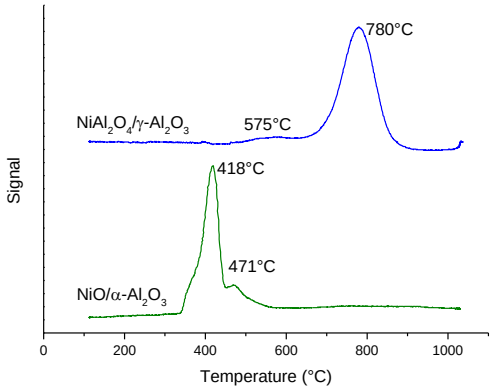

Figure 3. TPR analysis of the $NiO/\gamma\text{-}Al_2O_3$ and $NiAl_2O_4/\alpha\text{-}Al_2O_3$ oxygen carriers.

3.2. TGA Reactivity tests

Figure 4 shows thermogravimetry analysis of the two oxygen carriers. The duration of the reduction step was defined for the two materials from the moment that mass gain was observed. Thus the reduction times were defined as 1 minute for $NiO/\alpha\text{-}Al_2O_3$ and 4 minutes for $NiAl_2O_4/\gamma\text{-}Al_2O_3$, and oxidation time was defined as 2 minutes for both carriers, which was enough for total reoxidation. Table 2 shows the mass variations for cycles 2, 5, and 12 for both carriers. The stability of the behavior of both materials can be seen throughout the 12 cycles. Comparing the mass variation of the carriers with the Ni level results obtained by ICP, assuming it is in the form of NiO, consumption of oxygen contained within the carriers was 98.8% for $NiAl_2O_4/\gamma\text{-}Al_2O_3$ and 86.1% for $NiO/\alpha\text{-}Al_2O_3$.

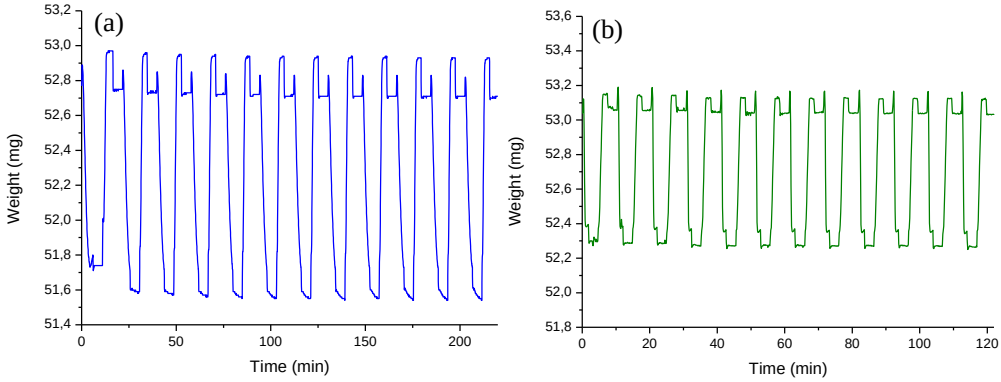

Figure 4. Redox cycles obtained by TGA of two oxygen carriers: (a) $NiAl_2O_4/\gamma\text{-}Al_2O_3$ and (b) $NiO/\alpha\text{-}Al_2O_3$.

Table 2. Weight variation of the $NiAl_2O_4/\gamma\text{-}Al_2O_3$ and $NiO/\alpha\text{-}Al_2O_3$ oxygen carriers for the 2nd, 5th and 12th cycles.

Carrier	$NiAl_2O_4/\gamma\text{-}Al_2O_3$	$NiO/\alpha\text{-}Al_2O_3$
Δm_2 (%)	2.20	1.45
Δm_5 (%)	2.20	1.46
Δm_{12} (%)	2.20	1.46

An important parameter that allows the behavior of the carriers to be evaluated during the redox cycles is conversion (ω) as a function of the material's total weight, defined by Equation 6.

$$\omega = \frac{m}{m_{ox}} \tag{6}$$

In which m is carrier weight at a defined moment during a reduction or oxidation step and m_{ox} is fully-oxidized carrier weight.

Using the results of the 5th cycle shown in Figure 4, it is possible to show carrier conversions ω, during the reduction or oxidation step (Figure 5). Figure 5a shows a higher reduction rate with the NiO/α-Al_2O_3 carrier than $NiAl_2O_4$/γ-Al_2O_3 carrier. The reduction time necessary to obtain the maximal oxygen consumption (86.1%) with the NiO/α-Al_2O_3 carrier was only 0.7 minutes, whereas at this same time oxygen consumption was 21% with the $NiAl_2O_4$/γ-Al_2O_3 carrier. These results confirm those obtained by TPR analysis (Figure 3), in which higher reducibility of free NiO can be seen than $NiAl_2O_4$, which agrees with other previously published results (Gayán et al., 2008). The oxidation rates observed with the two carriers were very high and almost the same (Figure 5b), leading to total oxidation in a short time.

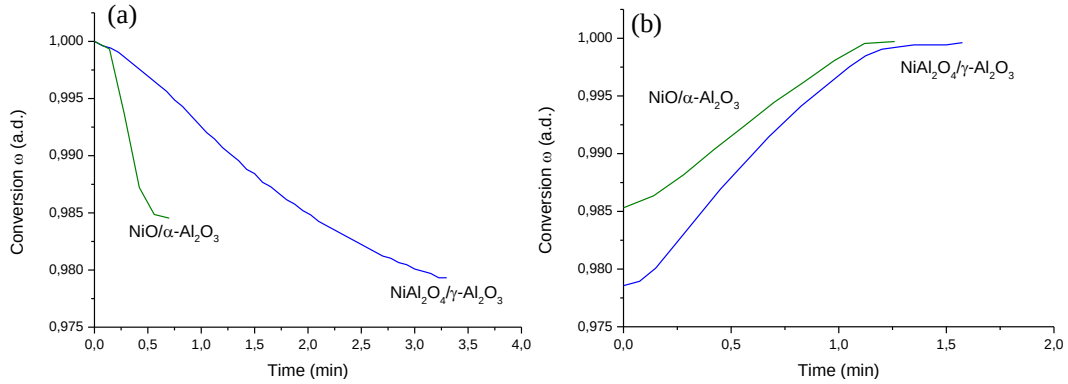

Figure 5. Conversion as a function of time for the fifth reduction (a) and oxidation (b) step for $NiAl_2O_4$/γ-Al_2O_3 and NiO/α-Al_2O_3 oxygen carriers.

3.3. Fixed bed batch tests

Figures 6a to 6d show the distribution of gas production during the redox tests carried out with NiO/α-Al_2O_3 and $NiAl_2O_4$/γ-Al_2O_3 oxygen carriers in a fixed bed reactor. Figure 6a shows the results of the 5th redox cycle of a sequence in which 10% CH_4 was utilized for 6 minutes in the NiO/α-Al_2O_3 reduction step. In this Figure, it can be noted the production of CO_2 and H_2O in the beginning of the step representing the reaction that characterizes the CLC process (Equation 1). After approximately 2 minutes of reduction, an increase in CO and H_2 production is observed at the same time as a drop in CO_2 production, suggesting that the CLR process (Equation 2) is more preferential. It can be seen also an excess of CH_4 after around 3 minutes of reaction, showing that there was no oxygen available in the carrier and that some of the catalytic sites were probably blocked by carbon deposits. The 4.1 H_2/CO ratio obtained by gas chromatography shows that hydrogen production was high, which could be attributed to the thermal and catalytic decomposition reaction of CH_4 (Equation 7), also causing carbon deposits on the surface of the carrier. These deposits could be confirmed in the oxidation step when high CO production is seen (Equation 8), in addition to a small amount of CO_2 (Equation 9). The level of carbon deposited in relation to CH_4, 22.2%, was estimated from areas of CO and CO_2 observed during the carrier oxidation step.

$$CH_4 \rightarrow 2H_2 + C \quad (7)$$

$$2C + O_2 \rightarrow 2CO \quad (8)$$

$$C + O_2 \rightarrow CO_2 \quad (9)$$

Figure 6b shows results of the 5th redox cycle of a sequence utilizing 5% CH_4 and 5% H_2O for 6 minutes in the NiO/α-Al_2O_3 reduction step. It can be noted in this Figure CO_2 and H_2O production until 3.2 minutes. H_2 and CO production is more common after this period. By the stoichiometry of the reaction, the H_2/CO ratio obtained in this period, 3.3, could indicate steam reforming of CH_4 (Equation 4), which demonstrates that the oxygen of the carrier is used less after 3.2 minutes. During the oxidation step, no CO or CO_2 is formed, indicating that no carbon is deposited.

$$CH_4 + H_2O \rightarrow CO + 3H_2 \quad (4)$$

Comparing Figures 6a and b, it can be noted that the utilization of H_2O in the reduction step was able to completely eliminate carbon deposits. The reduction of the H_2/CO ratio from 4.1 to 3.3 could also be attributed to utilization of H_2O during the reduction period, which could lead to the steam reforming of CH_4. In addition, with

utilization of H_2O, a greater amount of time was observed with a preference for production of CO_2 and H_2O, which could be attributed to the use of less CH_4 in this test.

Figures 6c and 6d shows distribution of gaseous production during redox tests carried out with the $NiAl_2O_4/\gamma$-Al_2O_3 carrier in a fixed bed reactor. Figure 6c shows results of the 5th cycle of a redox sequence in which 10% CH_4 was used for 5 minutes in the reduction step. It can be observed in this Figure CO_2 and H_2O production at the beginning of the reduction step, which quickly fell, with a greater preference for production of CO and H_2 starting at 0.8 minutes, much more quickly than seen for NiO/α-Al_2O_3. The methane was completely consumed during the reduction step, without an excess as seen with the NiO/α-Al_2O_3 carrier. All of the methane is consumed in 6 minutes of reaction due to the faster transition from the CLC to the CLR regime of this carrier, utilizing less of the oxygen carriers, as shown in the stoichiometry of Equation 2. The H_2/CO ratio obtained by gas chromatography, 2.8, again shows elevated H_2 production due to the thermal decomposition and catalytic reaction of methane. Carbon deposit can be confirmed too in the oxidation step, in which production of CO and CO_2 is observed. The level of carbon deposited in relation to CH_4, 15.4%, was also estimated by the areas of CO_2 seen in the oxidation step.

Figure 6d shows results from the 5th redox cycle of the $NiAl_2O_4/\gamma$-Al_2O_3 carrier carried out with 5% CH_4 and 5% H_2O in the reduction step. This figure shows behavior similar to that observed for the NiO/α-Al_2O_3 carrier analyzed in the same conditions. It can be noted a preference for the CO and H_2 production after 2 minutes of reaction. The H_2/CO ratio holds at 3.3, again showing that the main reaction from this point is steam reforming of methane. It can be observed a low level of CO and CO_2 production during the oxidation step, showing that addition of H_2O didn't prove to be as efficient as with the NiO/α-Al_2O_3 carrier, with 3.8% of the methane converted into carbon.

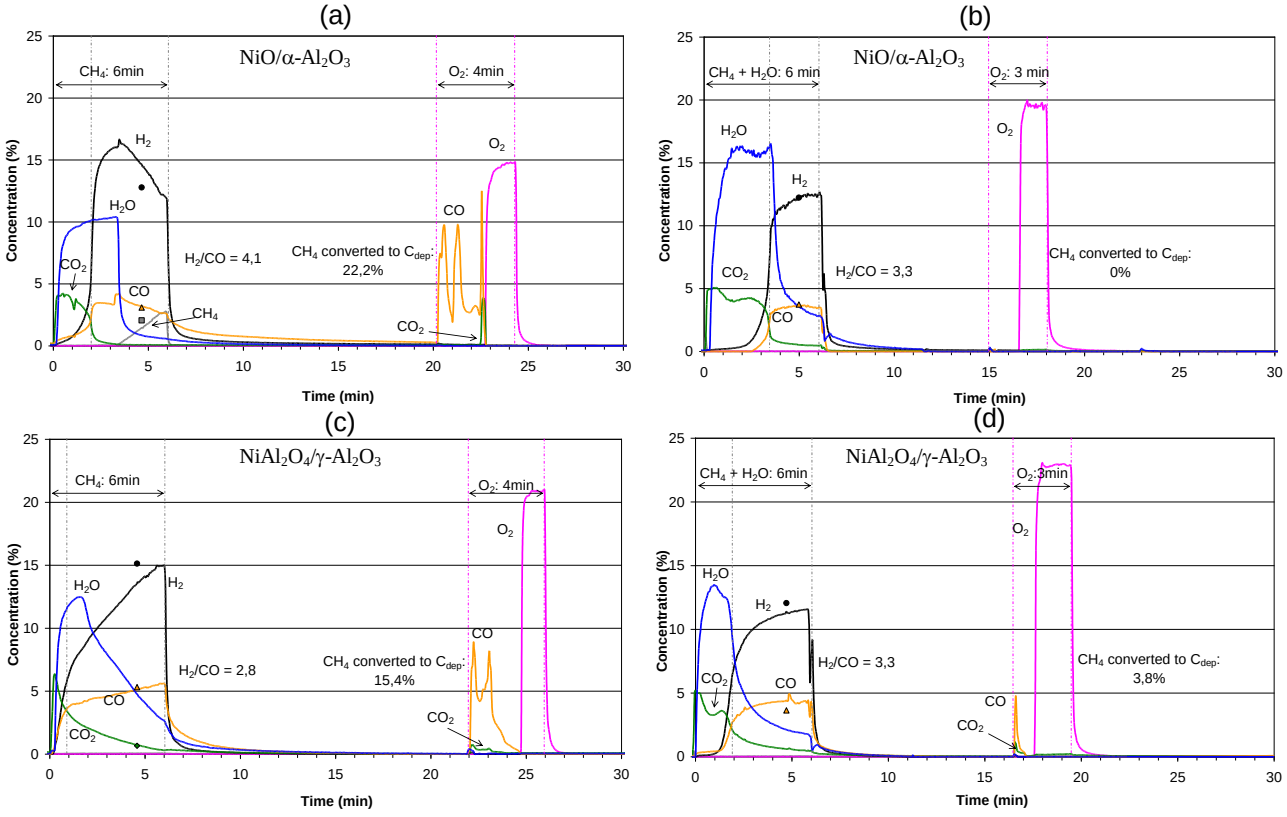

Figure 6. Gas product distribution measured during the 5th redox cycle in a fixed bed reactor at 950 ºC: (a) NiO/α-Al_2O_3 with 10% CH_4 , (b) NiO/α-Al_2O_3 with 5% CH_4 + 5% H_2O; (c) $NiAl_2O_4/\gamma$-Al_2O_3 with 10% CH_4 and (d) $NiAl_2O_4/\gamma$-Al_2O_3 with 5% CH_4 + 5% H_2O, measured by mass spectrometer. H_2 (●), CO (▲), CH_4 (■), CO_2 (◆) measured by gas chromatograph.

3.3.1. Effect of adding water

Keeping in mind that adding water to the reaction mixture in the reduction step has the effect of eliminating or reducing carbon deposits formed on the carrier, two reaction mechanisms were proposed that could explain the effect.

The first mechanism proposes that water reacts superficially with the reduced carrier, Me_xO_{y-1}, formed by CLC reactions (Equation 1) and/or CLR reactions (Equation 2), stopping the carbon from the methane thermal and catalytic decomposition reaction (Equation 7) from remaining on the surface of the carrier. Equation 10 shows the oxidation of the carrier with steam and Equation 11 shows the reverse reaction in which H_2 is again reduced to metallic oxide.

$$CH_4 + 4Me_xO_y \rightarrow CO_2 + 2H_2O + 4Me_xO_{y-1} \quad (1)$$
$$CH_4 + Me_xO_y \rightarrow CO + 2H_2 + Me_xO_{y-1} \quad (2)$$
$$Me_xO_{y-1} + H_2O \rightarrow Me_xO_y + H_2 \quad (10)$$
$$Me_xO_y + H_2 \rightarrow Me_xO_{y-1} + H_2O \quad (11)$$

The second mechanism proposes that CH_4 is dehydrogenated (Equation 7), generating carbon deposits, though the carbon is gasified when steam is added to the reaction medium (Equation 12). Equations 11 and 13 show the reduction of the metallic oxide by the H_2 and CO formed.

$$CH_4 + 4Me_xO_y \rightarrow CO_2 + 2H_2O + 4Me_xO_{y-1} \quad (1)$$
$$CH_4 + Me_xO_y \rightarrow CO + 2H_2 + Me_xO_{y-1} \quad (2)$$
$$CH_4 \rightarrow 2H_2 + C \quad (7)$$
$$C + H_2O \rightarrow CO + H_2 \quad (12)$$
$$Me_xO_y + H_2 \rightarrow Me_xO_{y-1} + H_2O \quad (11)$$
$$Me_xO_y + CO \rightarrow Me_xO_{y-1} + CO_2 \quad (13)$$

Gibbs free energies were calculated in function of the mechanisms proposed at 950 °C of both active phases present in the two oxygen carriers (NiO and $NiAl_2O_4$) in order to determine which could occur spontaneously at this temperature. Data provided by Lide (2001) and Barin (1995) were used for this purpose.

In addition to the Gibbs free energies of the steps involved in the first mechanism proposed, Table 3 shows the experimentally-obtained conversions for each of the steps after 15 minutes of reaction. Analyzing values obtained for NiO, the oxidation reaction of Ni^0 might not take place (Equation 10). According to Kang et al. (2010), ΔG° values above 25 kJ/mol might have low yield, while values between -25 and 25 kJ/mol represent reversible reactions, and values below -25 kJ/mol are typical of high yield reactions. Effectively, the results obtained in the laboratory with this reaction show that when there is steam present, only 7% of Ni^0 is converted to NiO after 15 minutes, which is totally incompatible with the results obtained previously shown in Figure 6. Consequently, the first mechanism can be discarded as a justification for the role of adding water in the behavior of products formed in the presence of the NiO/α-Al_2O_3 carrier. For the $NiAl_2O_4$ phase, note that the CLC reaction (Equation 1) has a very high ΔG° value, while the other three steps proposed have reversible reactions, which shows that this first mechanism can take place in the case of $NiAl_2O_4$.

Table 3. Standard Gibbs free energy at 950 °C for the first mechanism proposed.

Reactions	NiO		$NiAl_2O_4$	
	ΔG° (kJ/mol)	(%) Conversion	ΔG° (kJ/mol)	(%) Conversion
$CH_4 + 4Me_xO_y \rightarrow CO_2 + 2H_2O + 4Me_xO_{y-1}$	-290.11	-	187.86	-
$CH_4 + Me_xO_y \rightarrow CO + 2H_2 + Me_xO_{y-1}$	-136.10	-	-15.98	-
$Me_xO_{y-1} + H_2O \rightarrow Me_xO_y + H_2$	52.66	7	1.38	14
$Me_xO_y + H_2 \rightarrow Me_xO_{y-1} + H_2O$	-52.66	100	-1.38	27

In addition to the Gibbs free energies of the steps involved in the first mechanism proposed, Table 4 shows the experimentally obtained conversions for each of the steps after 15 minutes of reaction. For the NiO phase, ΔG° values are all negative, showing that the reactions could take place with high levels of conversion. For the $NiAl_2O_4$ phase, it can be noted that the second mechanism proposed could take place in function of the ΔG° values obtained, with the exception of the CLC reaction (Equation 1). Both active phase showed a high conversion to the carbon gasification by

steam reaction (Equation 12). Despite of this high conversion to the $NiAl_2O_4$ it was not obtained the complete carbon elimination as it can be observed at oxidation step (Figure 6d). This behavior possibly may be attributed to a most favorable kinetic of the methane catalytic decomposition (Equation 7) than the carbon gasification by steam reaction (Equation 12), considering the interaction between the carbon deposit with active phase $NiAl_2O_4$. In the same way theoretical ΔG^o values calculated also do not consider any carbon interaction with the active phase, since the values of $\Delta G°$ found in the literature, correspond to $NiAl_2O_4$ being reduced to Ni^0 and Al_2O_3.

Table 4. Standard Gibbs free energy at 950 °C for the second mechanism proposed.

Reactions	NiO		$NiAl_2O_4$	
	ΔG^o (kJ/mol)	(%) Conversion	ΔG^o (kJ/mol)	(%) Conversion
$CH_4 + 4Me_xO_y \rightarrow CO_2 + 2H_2O + 4Me_xO_{y-1}$	-290.11	-	187.86	-
$CH_4 + Me_xO_y \rightarrow CO + 2H_2 + Me_xO_{y-1}$	-136.10	-	-15.98	-
$CH_4 \rightarrow 2H_2 + C$	-43.82	-	-43.82	-
$C + H_2O \rightarrow CO + H_2$	-39.71*	100	-39.71*	100
$Me_xO_{y-1} + H_2 \rightarrow Me_xO_y + H_2O$	-52.66	100	-1.38	27
$Me_xO_y + CO \rightarrow Me_xO_{y-1} + CO_2$	-48.79	100	-34.00	6

*Carbon considered in its graphitic phase.

Tables 3 and 4 lead to the conclusion that for NiO, the second mechanism is more probable since all of the steps had high yield values. For $NiAl_2O_4$, both mechanisms are possible, though the theoretical values of some steps are in the range of $\Delta G°$ corresponding to reversible reactions, which could explain the fact that unlike the NiO/α-Al_2O_3 carrier, adding water didn't totally eliminate carbon deposits in the case of the $NiAl_2O_4$/γ-Al_2O_3 carrier.

4. Conclusions

The addition of Ni precursor ($Ni(NO_3)_2.6H_2O$) on two different alumina (α-Al_2O_3 and γ-Al_2O_3), lead to different oxygen carriers, after calcination treatment at 950 ºC. The material prepared on α-Al_2O_3 had only NiO and α-Al_2O_3 crystalline phases. With the material prepared on γ-Al_2O_3, the Ni precursor reacted with the support, generating the $NiAl_2O_4$ phase with two other crystalline phases, γ–Al_2O_3 and traces of NiO.

The addition of steam to CH_4 during the chemical-looping process has different effects when applied to NiO/α-Al_2O_3 than with $NiAl_2O_4$/γ-Al_2O_3. These behaviors can be explained by the mechanisms proposed in this work.

For NiO/α-Al_2O_3, results obtained by thermodynamical analysis and experimental tests carried out for each step showed that the main effect of steam was to react with the carbon deposit, generating CO and H_2, quickly and irreversibly, leading to the total elimination of carbon deposited on the carrier during the reduction step.

With the $NiAl_2O_4$/γ-Al_2O_3 carrier, using the same experimental methods, both of the mechanisms that have been proposed can be accepted. Both have less effective action of steam because reversible reactions are involved. These reversible reactions justify the incomplete removal of carbon deposited on this carrier during the reduction step.

5. Acknowledgments

The authors would like to thank to Petrobras S.A. for financial support and CNPq for scholarship support.

6. References

ABAD, A., ADÁNEZ, J., GARCÍA-LABIANO, F., DIEGO, L. F., GAYÁN, P., CELAYA, J. Mapping of the range of operational conditions for Cu-, Fe-, and Ni-based oxygen carriers in chemical-looping combustion. *Chemical Engineering Science*, v.62, p. 533-549, 2007.

ADANEZ, J., ABAD, A., GARCIA-LABIANO, F., GAYAN. P., DIEGO, L.F. Progress in chemical-looping combustion and reforming technologies. *Progress in Energy and Combustion Science*, v.38, p.218-282, 2012.

BARIN, I. Thermochemical data of pure substances. *VCH*. 3rd Edition. 1995.

CHO, P., MATTISSON, T., LYNGFELT, A. Comparison of iron-, nickel-, copper- and manganese-based oxygen carriers for chemical-looping combustion. *Fuel*, v. 83, p. 1215-1225, 2004.

CUNHA, P.; SANTAROSA, C.S. Desenvolvimento Tecnológico em Sequestro de Carbono na Petrobras, em Carbono: Desenvolvimento Tecnológico, Aplicação e Mercado Global. *Universidade Federal do Paraná*, 2006. p.274-279.

GAYÁN, P., DIEGO, L. F., GARCÍA-LABIANO, GAYÁN, P., ADÁNEZ, J., ABAD, A., DUESO, C. Effect of support on reactivity and selectivity of Ni-based oxygen carriers for chemical-looping combustion. *Fuel*, v. 87, p. 2641-2650, 2008.

GAYÁN, P., DUESO, C., ABAD, A., ADANEZ, J., DIEGO, L.F., GARCÍA-LABIANO, F. NiO/Al_2O_3 oxygen carriers for chemical-looping combustion prepared by impregnation and deposition-precipitation methos. Fuel, v. 88, p. 1016-1023, 2009.

KANG, K.S., KIM, C.H., BAE, K. K., CHO, W.C., KIM, S. H., PARK, C. S. Oxygen-carrier selection and thermal analysis of the chemical-looping process for hydrogen production. *International Journal of Hydrogen Energy*, v. 35 p. 12246-12254, 2010.

LIDE, D. R. CRC Handbook of Chemistry and Physics. *Chemical Rubber Company*. 82nd Edition. 2001.

LYNGFELT, A., LECKNER, B., MATTISSON, T. A fluidized-bed combustion process with inherent CO_2 separation; application of chemical-looping combustion. *Chemical Engineering Science*, v. 56, p. 3101-3113, 2001.

MATTISSON, T., JÄRDNÄS, A., LYNGFELT, A. Reactivity of some metal oxides supported on alumina with alternating methane and oxygen-application for chemical-looping combustion. *Energy & Fuels*, v. 17, p. 643-651, 2003.

RYDÉN, M., LYNGFELT, A., MATTISSON, T. Chemical-looping combustion and chemical-looping reforming in a circulating fluidized-bed reactor using Ni-based oxygen carriers. *Energy & Fuels*, v. 22, p. 2585-2597, 2008.

WALL, T., LIU, Y., MOGHTADERI, B. Chemical looping combustion and CO_2 capture. *Cooperative Research centre for coal in sustainable development*. The University of Newcastle, 2007.

ZAFAR, Q., MATTISSON, T., GEVERT, B. Redox investigation of some oxides of transition-state metals Ni, Cu, Fe and Mn supported on SiO_2 and $MgAl_2O_4$. *Energy & Fuels*, v. 20, p. 34-44, 2006.